Ultra-high area energy density of all-solid-state supercapacitor based on double-network hydrogel with high mass load

Liming Qin[1], Guiyan Yang[1], Dan Li[1], Kangtai Ou[1], Hengyu Zheng[1], Qiang Fu[2], Youyi Sun[1*]

1.Shanxi Province Key Laboratory of Functional Nanocomposites, North University of China, Taiyuan 030051, P.R. China.

2.School of Civil and Environmental Engineering, University of Technology Sydney, Ultimo NSW 2007, Australia.

Abstract: In order to improve the energy and power density of all-solid-state supercapacitor, more attention is currently focused on the development of electrodes and electrolyte materials with various chemical structure and/or compositions. However, current studies rarely report hydrogel electrodes with high loading content (i.e. >20.0wt%), and study their influence on the performance of supercapacitors. Here, we developed a novel double network, high loading content hydrogel material, and made it into electrode of all-solid-state supercapacitor by blade-coating and/or 3D printing. It is particularly worth noting that the resulting hydrogel electrode has an unusually high active material loading of 25.0wt% and exhibits ultra-high area specific capacitance (871.4mF cm^{-2}) and area energy density (143.1μWh cm^{-2} at 271.8μW cm^{-2} and 116.7μWh cm^{-2} at 1313μW cm^{-2}). This study therefore opens a new pathway for the development of high-performance all-solid-state supercapacitors on large-scale.

Keywords: high loading content, double network hydrogel electrode, 3D Printing, all-solid-state supercapacitor.

Responding author: Fax: 86-351-3559669

E-mail address: syyi@pku.edu.cn (YY Sun)

1. Introduction

Supercapacitor is a promising new energy storage device, which combines the advantages of high power of electric double layer capacitor and high energy of battery[1-2]. However, traditional supercapacitors are vulnerable to various mechanical deformations, leading to liquid leakage, chemical corrosion and other safety issues, which may cause irreversible damage to the function of the device and cannot meet the needs of flexible wearable electronic devices[2-3]. As an emerging class of supercapacitors, all-solid-state supercapacitor holds a great promise for energy storage and power supplies ascribing to its excellent safety and remarkable flexibility[4-8].The design, preparation and properties of electrode and electrolyte material are the key to improving the performance of flexible, all-solid-state supercapacitors[9-13]. Currently, the electrodes of supercapacitor are made of electrochemically active carbonaceous materials[14-15], transition metal oxides[16-17], conductive polymers (CPs)[18-20], and/or composites of above materials[21-22], and the electrolytes are usually polymer hydrogels containing H_2SO_4[23-24]. Among these materials, hydrogel is considered an ideal candidate owing to its flexible three-dimensional network, high deformability and high hydrophilicity. Hydrogel with high ion content can provide high ionic conductivity while maintaining its original shape and size, thereby reducing the risk of liquid leakage during various mechanical deformation processes[25]. In addition, the new hybrid hydrogels composed of electrochemically active materials and polymeric matrix have an inherent porous structure, excellent conductivity and flexibility[26]. Unfortunately, there are still research bottlenecks in the development of all-solid-state supercapacitors based on hydrogels. The high interfacial impedance between the current collector and the electrode results in a large electron transport and diffusion resistance from the electrode to the current collector. The incompatibility between

active materials and polymer matrix further limits the processability of such hydrogels. As a result, many high-performance active materials cannot be incorporated into hydrogel electrodes, and the loading content of suitable active materials is also limited to a low level. Therefore, it is still an ambitious challenge to develop a new strategy for fabricating all-solid-state supercapacitors with high loading and high performance.

In this study, we reported the development of a novel double network hydrogel, which was then used as an electrode material for assembling all-solid-state supercapacitors. We thus addressed the high interfacial impedance between electrode and current collector, improving the electron diffusion at interface. We further introduced a novel lyotropic liquid crystal into polyvinyl alcohol (PVA) hydrogel system to improve the polymer/filler compatibility, thereby increasing the loading of active materials. Through this strategy, we have prepared a series of hybrid hydrogel electrodes, which have high loading content of active materials, and all-solid-state supercapacitors with excellent areal energy density.

2. Experimental

2.1 Materials

Aniline (AN), ammonium persulfate (APS) and polyvinyl alcohol (PVA, degree of hydrolysis 99%, degree of polymerization 1788) were purchased from Shanghai Chemical Reagent Co., Ltd. Nitric acid (HNO_3) and hydrogen chloride (HCl) were purchased from Sinopharm Chemical Reagent Co., Ltd. Flake graphite was purchased from Nanjing Jiahui carbon Material Co., Ltd. Concentrated sulfuric acid (H_2SO_4) was purchased from Chengdu Cologne Chemical Reagent Co., Ltd. Phosphoric acid (H_3PO_4), sodium carbonate (Na_2CO_3) and sodium carbonate (Na_2CO_3) were purchased from Sinopharm Chemical Reagent Co., Ltd. Hydrogen peroxide (H_2O_2)

was purchased from Tianjin Damao Chemical Reagent Co., Ltd. Carbon cloth (CC, wos1009) was purchased from Tianjin Aiweixin Chemical Technology Co., Ltd. All reagents were used as they are without further purification.

2.2 Preparation of Graphene with high conductivity

Graphene was prepared by water-exfoliated method. Firstly, 30.0g $KMnO_4$ was added into 180.0mL concentrated sulfuric acid under mechanical stirring. 30.0g natural graphite was further added to above mixture. After mechanical stirring for 1.0h, 30.0g Na_2CO_3 was added. One hour later, 420.0mL H_3PO_4 was added into above mixture, and allowed for react for another 5.0 hours. Finally, the product was washed and filtered for three times, dispersed in 750mL NaOH solution (pH=14) and exfoliated in water under 15000 rpm mechanical stirring for 2h, yielding graphene dispersion solution.

2.3 Synthesis of polyaniline fiber

Polyaniline fiber was synthesized according to previous work[27]. 3.0mL aniline monomer and 1.8g ammonium persulfate were dissolved in 100.0mL hydrochloric acid (1M), respectively. The two solutions were mixed under mechanical stirring for 30s and then retained for 24h. Finally, the fiber dispersion solution was filtered, and the polyaniline nanofibers were washed by H_2O for three times, followed by freeze-drying.

2.4 Preparation of double network hydrogel

10.0g PVA and 90.0mL deionized water were stirred at 95.0℃ for 1.0h to obtain a transparent PVA aqueous solution. Then active materials (e.g. polyaniline fiber and

graphene, weight ratio = 4:1) were added into 3.0g PVA solution under stirring to form a uniform dispersion system. 0.5g triethanolamine and 1.0g oleic acid were added to above system under stirring (10min) to obtain a uniform gel precursor, and the gel precursor was centrifuged at 3000 rpm for 5.0min to remove air bubbles. The gel precursor was then frozen in a refrigerator at -20.0°C for 1.0 h, and then placed in a saturated boric acid solution for 12.0 h to obtain a stable double network hydrogel. Double network hydrogels with various contents (0, 5.0, 10.0, 20.0 and 25.0wt%) of active materials were prepared by the same method.

2.5 Fabrication of the all-solid-state supercapacitor

The all-solid-state supercapacitor based on double network hydrogel was fabricaed as shown in Scheme 1. The carbon cloth was immersed in HNO_3 (6.0M) at room temperature for 3.0 days, and then washed with deionized water and ethanol to improve its hydrophilicity. The obtained gel precursor (0.13g) was coated on the surface (1.0 cm×1.0 cm) of carbon cloth via blade casting. The carbon cloth coated with gel precursor was frozen in the refrigerator at -20.0°C. After 1.0h, it was removed and immersed in a saturated boric acid solution for 12.0h, affording hydrogel electrode. The electrodes were then immersed in H_2SO_4 solution (1 M) for 24h. 10.0g PVA powder was dissolved in 90.0g H_2SO_4 solution (1.0M) at 95°C, yielding PVA/H_2SO_4 gel electrolyte. The sandwiched all-solid supercapacitor consisting of two hydrogel electrodes and PVA/H_2SO_4 gel electrolyte was further assembled and sealed using plastic bag for long-term stability studies under environmental conditions.

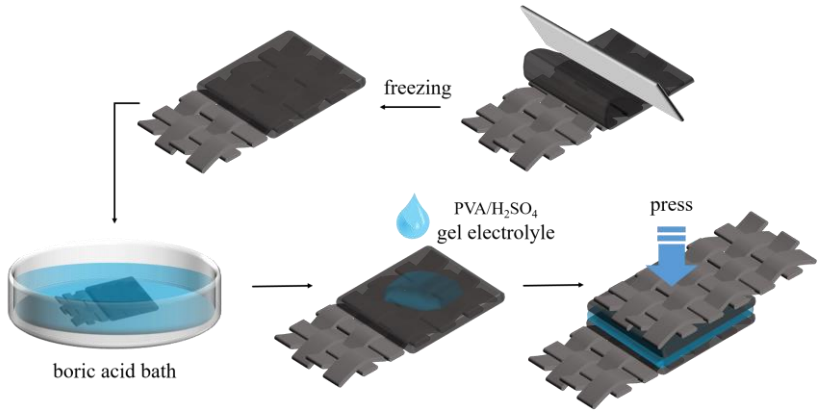

Scheme 1. Schematic illustration for preparation of all solid-state supercapacitors

2.6 Characterization

Morphology of double-network hydrogel under 5kV accelerating voltage was studied by scanning electron microscope (JSM-6700F).

The X-ray diffraction patterns of the liquid crystal phase were obtained by using Cu and Kα targets，tube current 40.0mA, tube voltage 40.0kV, continuous spectrum scanning, and scanning in the range of 1~5º.

Fourier transform infrared (FT-IR) spectroscopy of samples was measured by FT-IR analyzer (FTIR-8400s) at 4000~400cm^{-1}.

The liquid crystal phase was recorded by (Thermo Nicolet 360) spectrometer at room temperature.

2.7 Electrochemical performance of supercapacitor

Cyclic voltammetry (CV), constant current charge discharge (GCD) and electrochemical impedance spectra (EIS) of supercapacitor was recorded using a CHI660E workstation. The potential range of CV and frequency range of EIS are about -0.4～0.7V and 0.01 Hz~100.0 kHz, respectively. The scanning range and the current density of GCD are about -0.4~0.7V and 0.5mA/cm^2~2.5mA/cm^2, respectively. According to GCD data, the area capacitance (C_S, mF/cm^2), area energy density (E_S,

mWh/cm^2) and area power density (P_S, mW/cm^2) of single electrode materials can be calculated by the following formula[28-32]:

$$C_S = \frac{I\Delta t}{S\Delta V} \quad (1)$$

$$E_S = \frac{C_S \Delta V^2}{2} \quad (2)$$

$$P_S = \frac{E_S}{\Delta t} \quad (3)$$

Where I(A) is the discharge current, $\triangle t$ (s) is the discharge time, $\triangle V$ (V) is the voltage window (deducting the voltage drop), and S (cm^2)is the total area of the double electrodes of the device.

3. Results and Discussions

The hybrid, double-network hydrogel was composed of liquid crystal clusters and physical cross-linking network as shown in Fig.1A-B. The liquid crystal structure was constructed by mixing triethanolamine and oleic acid. As shown in Fig.1A, the N atom of triethanolamine can provide a lone pair of electrons and form acid-base complexes with oleic acid[33]. The resulting amphiphilic complexes would further self-assemble to micelles. When the concentration of micelle reaches its critical transition point, the mixture became gel (Fig.1A). The liquid crystal structure was confirmed by polarizing microscope, infrared spectroscopy and small-angle diffraction. As shown in Fig.1A-d, we observed irregular structure and a large number of extinction crosses under a polarized light microscope, suggesting liquid crystal structure[34]. sFig.1A shows the small-angle diffraction of the gel. A XRD peak at 2.3° reveals a typical highly ordered layered structure[35]. As shown in sFig.1B, the vibration absorption peak at 1715.32cm^{-1} assigned to C=O bond stretching of oleic

acid almost disappeared in the gel[36]. At the same time, a new absorption peak at 1563.36 cm^{-1} was observed. which belongs to the vibration absorption of N-H[37]. This result further confirmed the formation of liquid crystal structure caused by the interaction between C=O of oleic acid and N of triethanolamine. The gelation of the mixture can be attributed to the hydrogen bonding between -OH of liquid crystal (LC) structure and H atom of H_2O molecules. Moreover, the resulting LC gel has unique characteristics, which were rarely observed in previous studies[38-39]. Specifically, this LC gel system shows excellent compatibility with various electrochemical active materials (i.e. graphene, PANI, etc), thereby enhancing the loading of active materials in the LC gel system. This can effectively improve the area or volume energy density of an all-solid-state supercapacitor assembly. However, such hydrogel system showed poor stability in H_2SO_4 electrolyte (in sFig.2B-a). To address this issue, the second polymeric network is incorporated into this gel system facilitated by graphene and PANI (Fig.1B). Specifically, a mixture containing PVA, graphene and PANI was feezed, inducing PVA crystallization and phase separation. Through van der Waals force and intra-/inter-molecular hydrogen bonding, the PVA chains form compact colloids. Before the colloid thaw, the frozen gel was immersed into boric acid. The esterification/cross-linking between –OH groups of PVA and boric acids occurred, yielding stable hydrogel. The network composed of PVA, graphene, PANI and boric acid was also characterized by IR and Raman spectroscopies (in sFig.3). As shown in sFig.3A, the peak at 2910.0cm^{-1} was assigned to the vibrational absorption of the –CH_2 of PVA[32]. After gelation, a new peak at 1410cm^{-1} was also observed, which was

assigned to the stretching vibrations of borate ester bond, indicating the formation of cross-linking[40]. As shown in sFig.3B, the Reman absorption peaks at 2912.0 and 1430.0 cm^{-1} were assigned to -CH_2 stretching vibration of PVA and borate ester, respectively[41]. In addition, the two characteristic bands of 1347.5 and 1593 cm^{-1} were also observed, which were assigned to D-and G-band of graphene, respectively[32]. We further demonstrated that the introduction of PVA secondary network can provide extra stability in H_2SO_4 electrolyte and restrict the dissolution of graphene and PANI from LC gel system (Fig.1C, and sFig2B-b) Thus, we can conclude that the construction of double-network hydrogel containing PANI and graphene is the key to prepare stable electrodes.

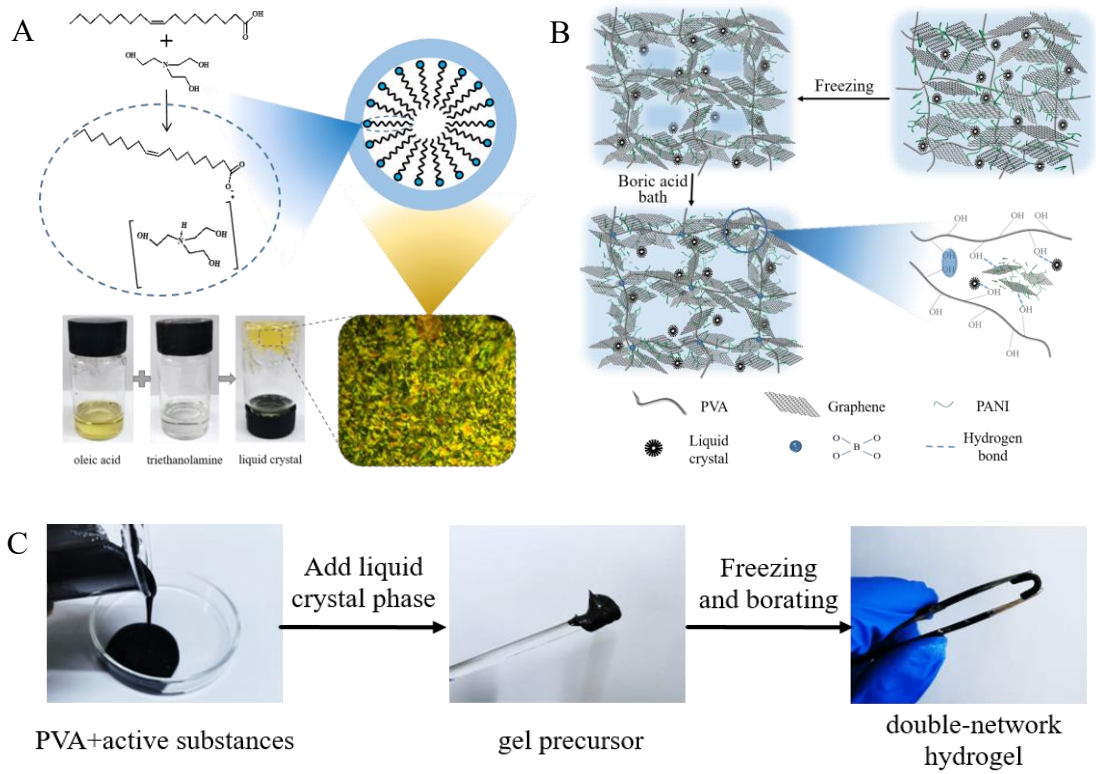

Fig.1. Schematic illustration of double-network hydrogel. (A) Photo comparison: (a) PVA has fluidity after adding active substances, (b) after adding liquid crystal phase

into PVA, the coating slurry will lose its fluidity, (c) double-network hydrogel after soaking in boric acid and curing. (B)Schematic diagram of the liquid crystal structure (C)Optical photo of forming process.

The microstructure of the double-network hydrogel electrode was characterized by SEM measurements and the images are shown in Fig.2. We clearly observed fiber and flake structure of the prepared active materials PANI and graphene in Fig.2A and 2B, respectively. As shown in Fig.2C and 2D (enlarged SEM image), the double-network hydrogel exhibits a porous structure, providing a large electrochemical active surface area and a low ion transport and diffusion resistance from electrolyte to electrode materials. The graphene nanosheets were uniformly dispersed in double-network and contacted with each other, forming a continuous conductive network with high conductivity of ca.168.3 S/m). The high conductivity of electrode can be attributed to the high conductivity (ca.~10^4 S/m) of graphene. Fig.2E-F shows the cross-section SEM images of the double-network hydrogel. The double-network closely coated on and penetrated into the carbon cloth, which is rarely reported in previous literature[4, 10, 41]. These features are important for reducing electron resistance and mitigating shift distance from electrode to current collector. These results demonstrate the successful preparation of double-network hydrogels with porous structure, high conductivity and low interface resistance.

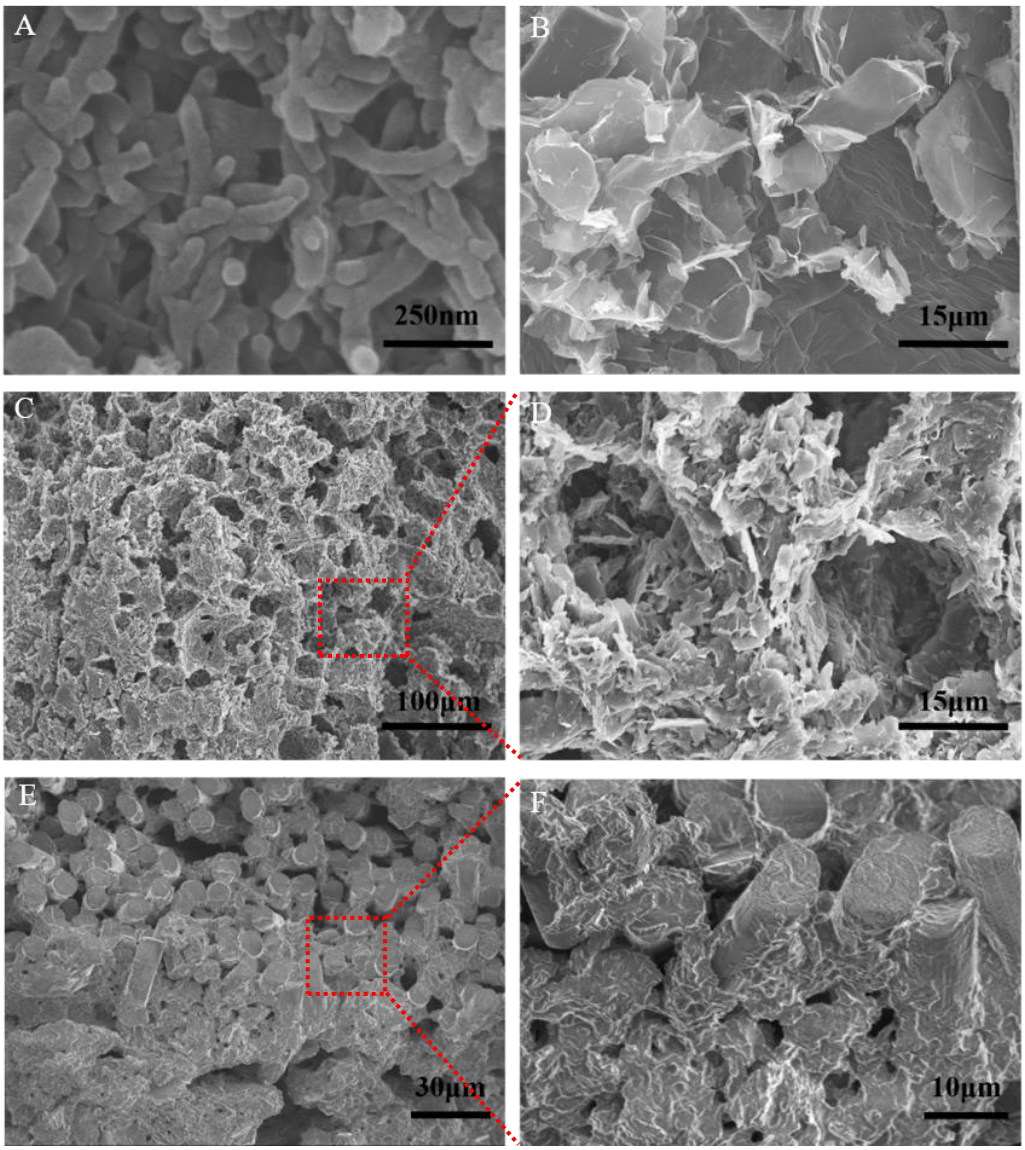

Fig.2. SEM images of (A) PANI and (B) graphene. (C-D) Surface and (E-F) cross-section SEM images of double-network hydrogel.

The electrochemical performance of the assembled supercapacitor was tested using an electrochemical workstation. The CV curves of the supercapacitors with various contents of active materials were recorded at a scanning rate of 100 mV/s (Fig.3A). All the CV curves were nearly rectangular and symmetrical, indicating excellent electrochemical reversibility and high capacitive performance. Among these samples, the supercapacitor with 25.0wt% active material shows the largest specific

capacitance. In addition, the CV areas increased with increasing the content of active materials, indicating enhanced specific capacitance of supercapacitor. Fig.3B shows the CV curves of the hydrogel supercapacitor with 25.0wt% active materials as a function of scanning rates from 20 to 100 mV/s. Enhanced current response and nearly rectangular CV profiles were observed at high scanning rate, indicating excellent rate performance and ideal capacitance behavior. This result also reveals the highly porous structure of hydrogel and excellent compatibility between organic matrix and carbon fiber. In addition, the CV curves could maintain the shuttle shape and high symmetry, indicating double-layer capacitance characteristics and high coulomb efficiency[4, 42].

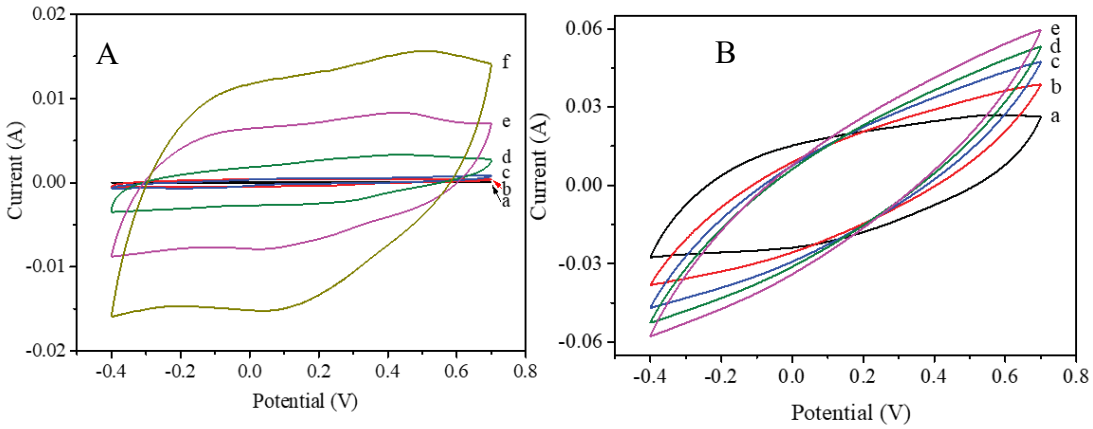

Fig.3. (A) CV curves of assembled hydrogel supercapacitors with different active materials loading: (a) 0, (b)5.0wt%, (c)10.0wt%, (d)15.0wt%, (e) 20.0wt % and (f) 25.0wt% at 10.0mV/s. (B) CV curves of the hydrogel supercapacitor with 25.0wt% active materials loading as a function of scanning rate from 20 to 100mV/s.

Fig.4A shows the constant current charge discharge (GCD) behavior of the present supercapacitor at a current density of 0.5mA/cm^2. The GCD curves of all samples were nearly symmetrical triangles, indicating a typical double-layer

capacitance again[43]. In addition, we found that that the supercapacitor with 25.0wt% active materials displays the longest discharge time, which means the largest special capacitance. We also observed that when the loading content of active material in hydrogels increased from 0 to 25.0wt%, the area specific capacitance of corresponding supercapacitors sharply increased from 6.9 to 871.4mF/cm^2 (Fig.1B). Fig.4C shows the GCD curves of the double-network supercapacitor with 25.0wt% active materials as a function of current density. When the current density increased from 0.5 to 2.5mA/cm^2, all curves maintain their symmetrical shape of an isosceles triangle. As shown in Fig.4D, when the current density increased from 0.5 to 2.5 mA/cm^2, the area specific capacitance of the supercapacitor slightly decreased from 871.4 to 761.6 mF/cm^2. At the same time, although the current density has increased by 5 times, the area capacity retention dropped by about 13.0%. These results further confirmed that the double-network hydrogel with high mass loading displayed the best rate performance compared to other supercapacitor counterparts.

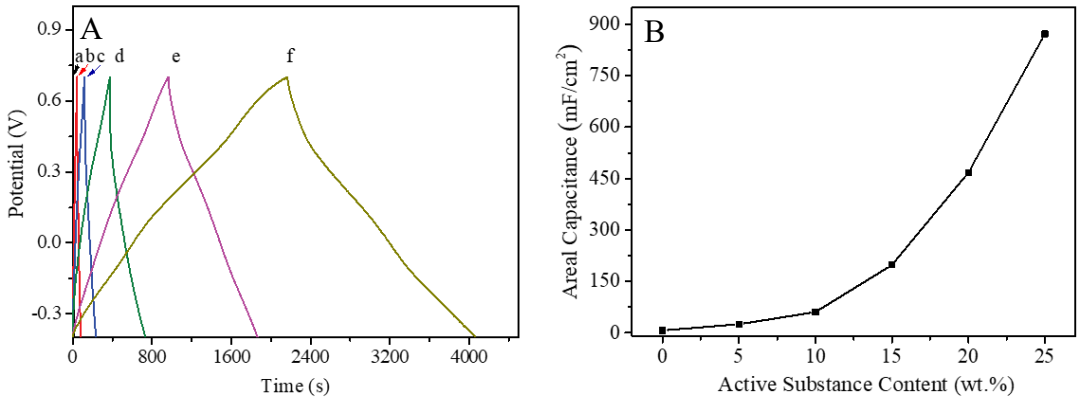

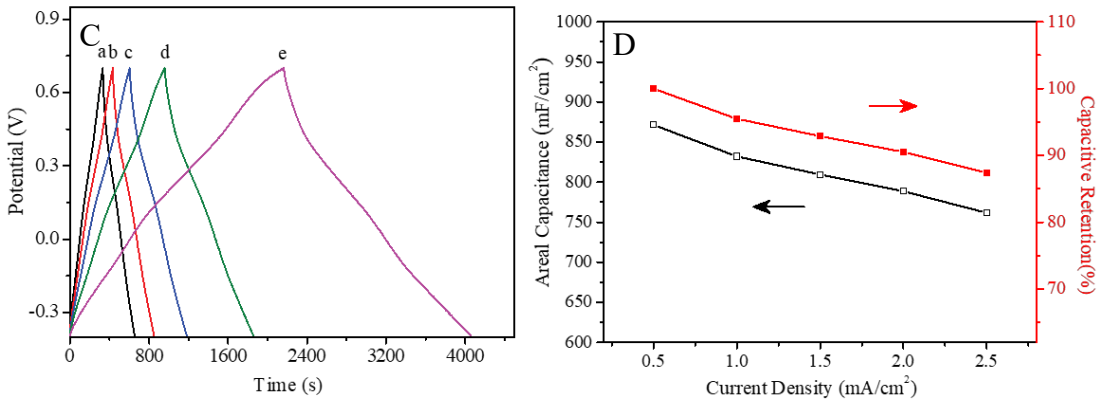

Fig.4. (A) GCD curves and (B) area specific capacitance of the double-network hydrogel supercapacitors with various loading contents of active materials, (a) 0, (b)5.0wt%, (c)10.0wt%, (d)15.0wt%, (e)20.0wt% and (f) 25.0wt%. (C) GCD curves and (D) area specific capacitance of the supercapacitors as a function of current densities from 0.5 to 2.5mA/cm^2.

The cyclic stability of the prepared supercapacitor with high mass loading was further evaluated and the results are shown in Fig.5A. At a current density of 2.5mA/cm2, the supercapacitor can still maintain a high area specific capacitance of 832.5mF/cm^2 and a capacity retention rate of up to 95.6% after 1000 charge/discharge cycles, showing outstanding cyclic stability. The area energy density and power density of supercapacitor at various current densities were calculated and compared with the results reported in previous literature[42, 44-49] (Fig.5B). When the current density increased from 0.5 to 2.5mA/cm^2, the area energy density of supercapacitor slightly decreased from 0.14 to 0.12mWh/cm^2 in the range of area power density from 0.27 and 1.31mW/cm^2. As shown in Table 1, the present supercapacitor shows the largest area special capacity and area energy density in comparison with others

supercapacitors reported in previous literature [2, 4, 40-43, 48-51]. In Fig.5C, we demonstrated the all-solid-state supercapacitors can work as a power supply unit and light up a red LED. These results further confirmed the excellent electrochemical performance of the all-solid-state supercapacitor based on double-network hydrogel electrode, which has a high mass loading of active materials, and showed its potential in practical energy storage applications.

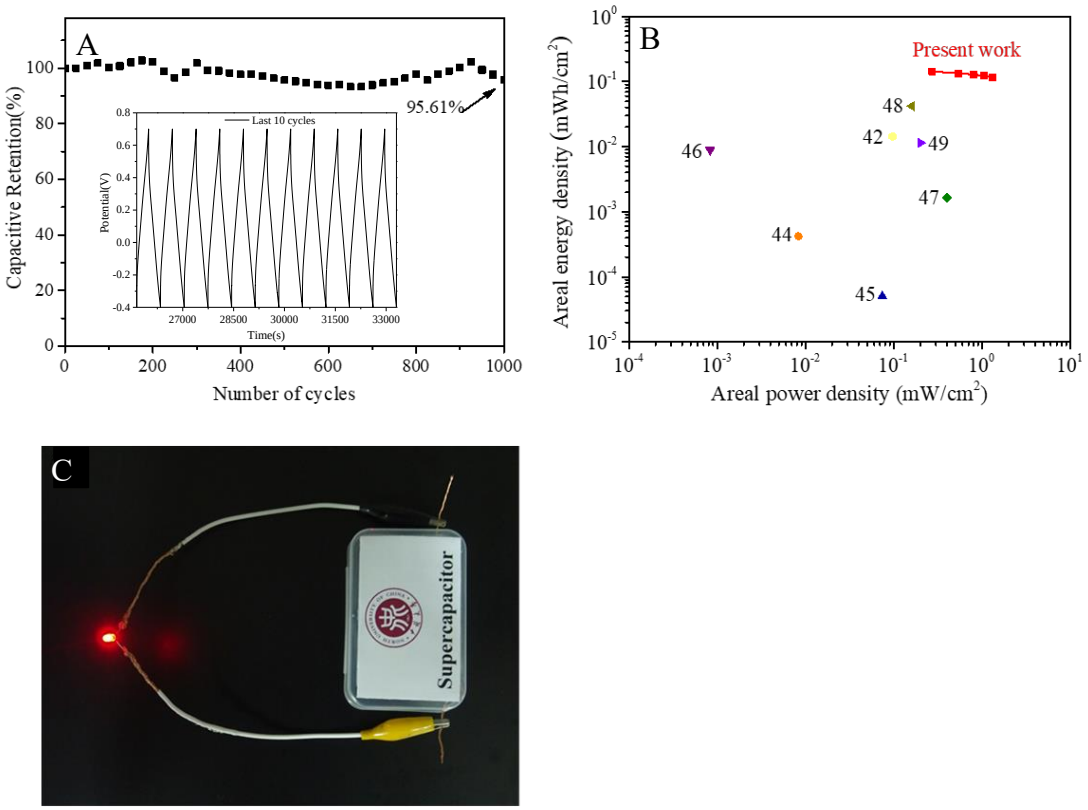

Fig.5. (A) The capacity retention of double-network hydrogel supercapacitor with high mass loading as a function of charge/discharge cycles. (B) The area energy density *vs.* area power density of supercapacitors (this work compared to previous literature) at different current densities. (C) The photo image of supercapacitor serving as a power supply for a red LED.

Table 1. Structure and electrochemical performance of the supercapacitors reported in previous literature and in this work.

Reference	Active materials	Content	Areal Capacitance	Cycle stability
Present	G/PANI	25.0wt% ($32.5mg/cm^2$)	871.4 mF cm^{-2} (0.5 mA cm^{-2})	95.6% (1000)
[2]	CNT@PANI	<0.1wt%	138 F/g (at 0.6 A/g)	86% (1000)
[4]	GO/PEDOT	$0.87mg/cm^2$	75.9 F/g (0.29 A/g)	89% (1000)
[40]	PANI/G	<10.0wt%	344.8 mF cm^{-2} (0.3 mA cm^{-2})	84.3% (3000)
[41]	PPy/MXene	0.49 mg/cm^2	614.0F/g a	83% (1000)
[42]	PANI/CNTs	4.8wt%	169.3 mF cm^{-2} (0.25 mA cm^{-2})	97.5% (1000)
[43]	PPy	11.0wt%	103.3 F g^{-1}	84% (10000)
[48]	PANI	5.76 mg/cm^2	488 mF cm^{-2}	99% (7000)
[49]	PEDOT:PSS	<1.3wt%	128.9 mF cm^{-2}	89.8% (10000)
[50]	PANI	<5.0wt%	151.9 mF cm^{-2}	79.5% (5000)
[51]	PANI	<8.3wt%	11.3 mF cm^{-2} (5 mV s^{-1})	83.3% (1000)

The charge transfer and ion diffusion resistance at electrolyte/electrode/current collector interfaces were further investigated by the EIS spectra as shown in Fig.6.

When the active materials loading content increased from 0 to 25.0wt%, the equivalent series resistance (ESR) of the double-network supercapacitors reduced from 12.5 to 2.5Ω (Fig. 6A, insert). Lower ESR indicated lower internal resistance and lower charge transfer resistance, indicating enhanced electrochemical performance. The result can be attributed to good conductivity of graphene and improved interfacial contact between hydrogel electrode and current collector. We did not observe the semicircle in the high-to-medium frequency region. This result indicates a low ion diffusion resistance from electrode material to current collector. In addition, the slope of the straight line in the low frequency region increased when increasing active materials loading content. This discloses that conductive network is gradually connected with the increase of active substances, providing a good pathway for rapid ion exchange and/or ion diffusion. The enhanced electrochemical performance of the supercapacitors can be attributed to the reduced internal resistance and ion diffusion resistance caused by incorporating more active materials into the double-network.

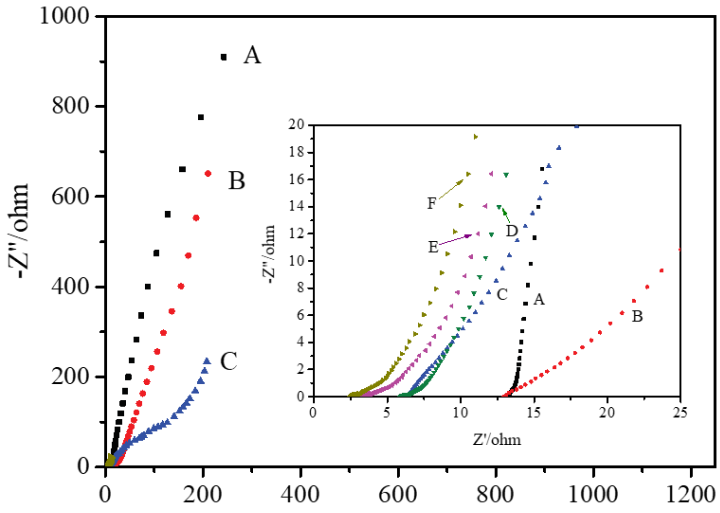

Fig.6. EIS spectra of the double-network supercapacitors with various active materials loading contents (A)0, (B)5.0wt%, (C)10.0wt%, (D)15.0wt%, (E)20.0wt%, and (F) 25.0wt%.

We then investigate the rheological properties of the gel precursors before cross-linking and evaluate their 3D printing ability. In Fig.7A, it can be seen that the apparent viscosity of the gel precursor decreased with the increase of shear rate, indicating a shear thinning effect. Through the dynamic mechanical properties testing (Fig.7B), we also found that the storage modulus of gel precursor is lower than that of loss modulus at a lower shear stress of 100.0Pa, indicating a gel character. These results confirmed the excellent printing ability of the gel precursor: namely shear thinning effect and high modulus. After immersion in boric acid, the mechanical stability of the 3D printing structures could be further enhanced. Therefore, we can introduce a significant amount of active materials into the printing ink (gel precursor) and prepare 3D printed electrodes by solving current limitations in this field.

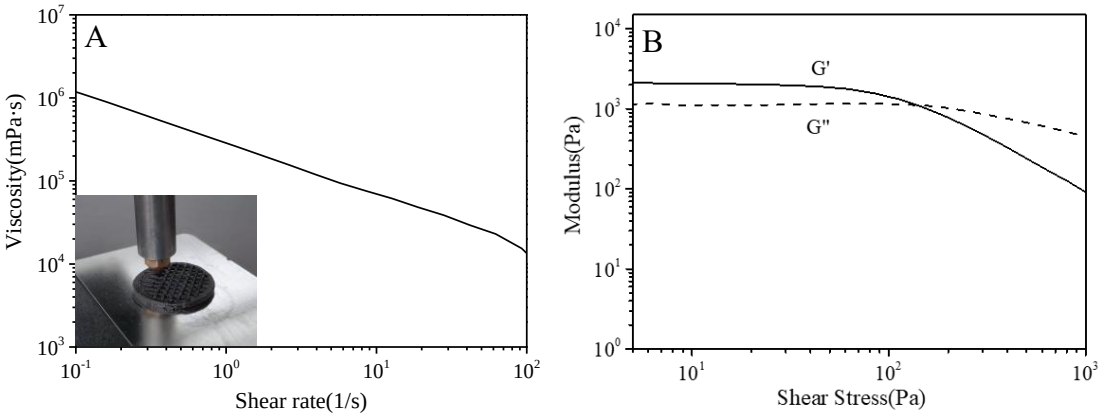

Fig.7. The rheological properties of gel precursors as 3D printing ink. (A) The apparent viscosity of gel precursors *vs.* the shear rate. (B) The storage modulus and loss modulus of gel precursors *vs.* shear stress.

We used the gel precursor with active substance loading content of 20.0wt% as 3D printing ink to prepare electrodes on the carbon cloth. After freezing and borating, the sandwich all-solid-supercapacitors were assembled (Fig.8). The electrochemical performance of 3D printing all-solid-supercapacitors was characterized and the results are shown in Fig.8A-C. The 3D printing supercapacitors showed identical electrochemical performance compared to the blade-coating counterparts. At the current density of 0.5 mA/cm^2, the area specific capacitance of the device reaches 483.9mF/cm^2. When the current density increases to 2.5mA/cm^2, the area energy density reaches 68.2 and 19.4μWh/cm^2, corresponding to area power density of 2511.9 and 1058.2μW/cm^2, respectively. However, we observed larger equivalent series resistance and diffusion resistance compared to the supercapacitors prepared via blade coating. This is because the 3D printing technique will inevitably lead to the anisotropy of the gel printed on surface of carbon cloth. The 3D printed solid-state supercapacitors can also work as a power supply unit and light up a yellow LED (Fig. 8D).

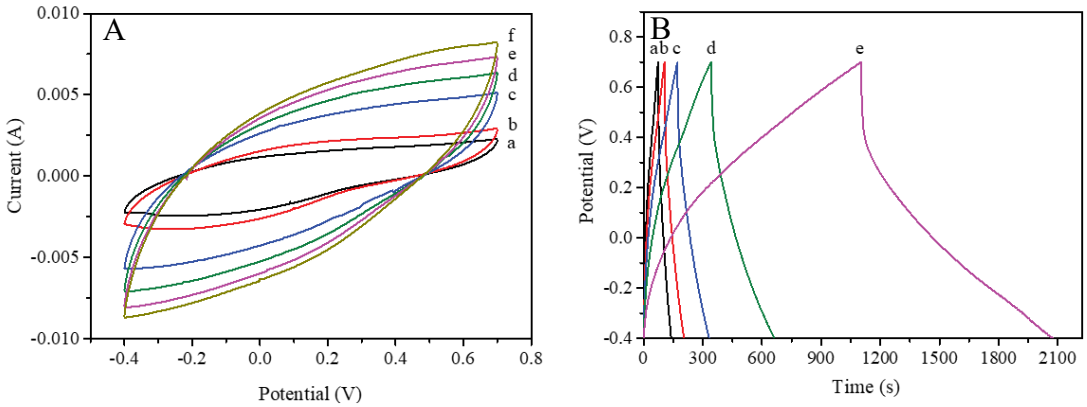

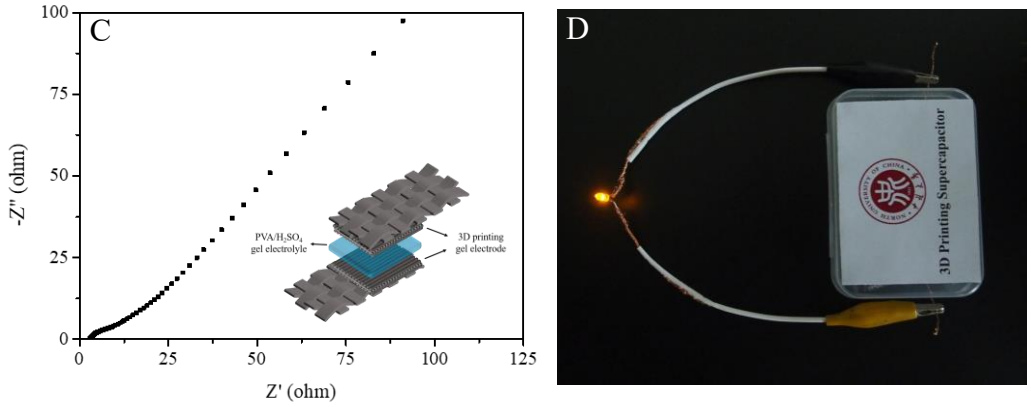

Fig.8. (A) The CV curves of 3D printed all-solid-state supercapacitors at different scanning rates of (a) 10.0mV/s, (b) 20.0mV/s, (c) 40.0mV/s, (d) 60.0mV/s, (e) 80.0 mV/s and (f) 100.0mV/s. (B) GCD curves under different current densities of (a) 0.5mA/cm^2, (b) 1.0mA/cm^2, (c) 1.5mA/cm^2, (d) 2.0mA/cm^2 and (e) 2.5mA/cm^2. (C) EIS data of 3D printed all-solid-state supercapacitors. (D) The photograph of 3D printed all-solid-state supercapacitors as a power supply unit.

4.Conclusions

In summary, we have developed a novel double-network gel system, which has enhanced compatibility with active materials. We then assembled hydrogel electrodes into all-solid-state, flexible supercapacitors. In addition, the gel precursors also displayed good printability and can be used as an ink material for 3D printing supercapacitors. Both of the supercapacitors we prepared showed high electrochemical performance and high stability. This study thus provides a new strategy for large-scale fabrication of high performance all-solid-state supercapacitors for practical applications.

Acknowledgment

Liming Qin and Guiyan Yang contributed equally to this work. The authors are grateful for the support of the National Natural Science Foundation of China under

grants (51773184 and U1810114), Shanxi Provincial Natural Science Foundation of China (201803D421081 and 201801D121104).

References

[1] Chen C R, Qin H, Cong H P, et al. A Highly Stretchable and Real-Time Healable Supercapacitor [J]. Adv Mater, 2019, 31(19): 1900573.

[2] Wang H, Biswas S K, Zhu S, et al. Self-Healable Electro-Conductive Hydrogels Based on Core-Shell Structured Nanocellulose/Carbon Nanotubes Hybrids for Use as Flexible Supercapacitors [J]. Nanomaterials (Basel), 2020, 10(1): 112.

[3] Sun X, Cai M, Chen L, et al. Electrodes of carbonized MWCNT-cellulose paper for supercapacitor [J]. Journal of Nanoparticle Research, 2017, 19(7): 239.

[4] Chen Q, Lu H, Chen F, et al. Supramolecular Hydrogels for High-Voltage and Neutral-pH Flexible Supercapacitors [J]. ACS Applied Energy Materials, 2018, 1(8): 4261-4268.

[5] Han Z, Xia T, Xu S, et al. A Study of All-solid-state Planar Micro-supercapacitors Using Printable MoS_2 Inks [J]. Chemistry Letters, 2021, 50(3): 452-455.

[6] Wang S, Tan C, Fei L, et al. Rational Design and in-situ Synthesis of Ultra-Thin beta-$Ni(OH)_2$ Nanoplates for High Performance All-Solid-State Flexible Supercapacitors [J]. Frontiers in Chemistry, 2020, 8.

[7] Yang Y. A mini-review: emerging all-solid-state energy storage electrode materials for flexible devices [J]. Nanoscale, 2020, 12(6): 3560-3573.

[8] Xie J, Sun X, Zhang N, et al. Layer-by-layer beta-$Ni(OH)_2$/graphene nanohybrids for ultraflexible all-solid-state thin-film supercapacitors with high electrochemical performance [J]. Nano Energy, 2013, 2(1): 65-74.

[9] Wang C, Yang Y, Li R, et al. Polyaniline functionalized reduced graphene oxide/carbon nanotube ternary nanocomposite as a supercapacitor electrode [J]. Chem

Commun (Camb), 2020, 56(28): 4003-4006.

[10]Dhibar S, Malik S. Morphological Modulation of Conducting Polymer Nanocomposites with Nickel Cobaltite/Reduced Graphene Oxide and Their Subtle Effects on the Capacitive Behaviors [J]. ACS Appl Mater Interfaces, 2020, 12(48): 54053−54067.

[11]Mao X, Zou Y, Xu F, et al. Three-Dimensional Self-Supporting Ti_3C_2 with MoS_2 and Cu_2O Nanocrystals for High-Performance Flexible Supercapacitors [J]. ACS applied materials & interfaces, 2021, 13(19): 22664-22675.

[12]Shewale P S, Yun K-S. $NiCo_2O_4$/RGO Hybrid Nanostructures on Surface-Modified Ni Core for Flexible Wire-Shaped Supercapacitor [J]. Nanomaterials, 2021, 11(4).

[13]Liu Z, Zhang J, Liu J, et al. Highly compressible and superior low temperature tolerant supercapacitors based on dual chemically crosslinked PVA hydrogel electrolytes [J]. Journal of Materials Chemistry A, 2020, 8(13): 6219-6228.

[14]Yu J, Wu J, Wang H, et al. Metallic Fabrics as the Current Collector for High-Performance Graphene-Based Flexible Solid-State Supercapacitor [J]. Acs Applied Materials & Interfaces, 2016, 8(7): 4724-4729.

[15]Chen T, Hao R, Peng H, et al. High-Performance, Stretchable, Wire-Shaped Supercapacitors [J]. Angewandte Chemie-International Edition, 2015, 54(2): 618-622.

[16]Shen L, Du L, Tan S, et al. Flexible electrochromic supercapacitor hybrid electrodes based on tungsten oxide films and silver nanowires [J]. Chemical Communications, 2016, 52(37): 6296-6299.

[17]Yang H, Xu H, Li M, et al. Assembly of NiO/Ni(OH)(2)/PEDOT Nanocomposites on Contra Wires for Fiber-Shaped Flexible Asymmetric Supercapacitors [J]. Acs Applied Materials & Interfaces, 2016, 8(3): 1774-1779.

[18]D'Arcy J M, El-Kady M F, Khine P P, et al. Vapor-Phase Polymerization of Nanofibrillar Poly(3,4-ethylenedioxythiophene) for Supercapacitors [J]. Acs Nano, 2014, 8(2): 1500-1510.

[19]Nyholm L, Nystrom G, Mihranyan A, et al. Toward Flexible Polymer and Paper-Based Energy Storage Devices [J]. Advanced Materials, 2011, 23(33): 3751-3769.

[20]Yuan L, Yao B, Hu B, et al. Polypyrrole-coated paper for flexible solid-state energy storage [J]. Energy & Environmental Science, 2013, 6(2): 470-476.

[21]Cho S, Kim M, Jang J. Screen-Printable and Flexible RuO2 Nanoparticle-Decorated PEDOT:PSS/Graphene Nanocomposite with Enhanced Electrical and Electrochemical Performances for High-Capacity Supercapacitor [J]. Acs Applied Materials & Interfaces, 2015, 7(19): 10213-10227.

[22]Tang P, Han L, Zhang L. Facile synthesis of graphite/PEDOT/MnO_2 composites on commercial supercapacitor separator membranes as flexible and high-performance supercapacitor electrodes [J]. ACS Appl Mater Interfaces, 2014, 6(13): 10506-10515.

[23]Cheng T, Zhang Y-Z, Zhang J-D, et al. High-performance free-standing PEDOT: PSS electrodes for flexible and transparent all-solid-state supercapacitors [J]. Journal of Materials Chemistry A, 2016, 4(27): 10493-10499.

[24]Kurra N, Wang R, Alshareef H N. All conducting polymer electrodes for asymmetric solid-state supercapacitors [J]. Journal of Materials Chemistry A, 2015, 3(14): 7368-7374.

[25]Huang Y, Zhong M, Shi F, et al. An Intrinsically Stretchable and Compressible Supercapacitor Containing a Polyacrylamide Hydrogel Electrolyte [J]. Angewandte Chemie-International Edition, 2017, 56(31): 9141-9145.

[26]Shi Y, Zhang J, Bruck A M, et al. A Tunable 3D Nanostructured Conductive Gel

Framework Electrode for High-Performance Lithium Ion Batteries [J]. Advanced Materials, 2017, 29(22).

[27]Kavitha B, Kumar K S, Narsimlu N. Synthesis and characterization of polyaniline nano-fibers [J]. Indian Journal of Pure & Applied Physics, 2013, 51(3): 207-209.

[28]Zhang G, Chen Y, Deng Y, et al. A Triblock Copolymer Design Leads to Robust Hybrid Hydrogels for High-Performance Flexible Supercapacitors [J]. ACS Appl Mater Interfaces, 2017, 9(41): 36301-36310.

[29]Zang L, Liu Q, Qiu J, et al. Design and Fabrication of an All-Solid-State Polymer Supercapacitor with Highly Mechanical Flexibility Based on Polypyrrole Hydrogel [J]. ACS Appl Mater Interfaces, 2017, 9(39): 33941-33947.

[30]Heydari H, Gholivand M B. An all-solid-state asymmetric device based on a polyaniline hydrogel for a high energy flexible supercapacitor [J]. New Journal of Chemistry, 2017, 41(1): 237-244.

[31]Li W, Li M, Bolton J R, et al. Configuration optimization of UV reactors for water disinfection with computational fluid dynamics: Feasibility of using particle minimum UV dose as a performance indicator [J]. Chemical Engineering Journal, 2016, 306.

[32]G.Z. Guo, Y.Y. Sun, Q. Fu , Y.B. Ma , Y.Y.Zhou , Z.Y.Xiong , Y.Y. Liu. Sol-gel synthesis of ternary conducting polymer hydrogel for application in all-solid-state flexible supercapacitor.pdf [J]. INTERNATIONAL JOURNAL OF HYDROGEN ENERGY ,2019, 44(12): 6103-6115.

[33]Stig E. Friberg P L. Slngle Compound Forming a Lyotropic Liquid Crystal at Room Temperature [J]. The Journal of Physical Chemistry B, 1984, 88(5): 1045-1046.

[34]Wychowaniec J K, Iliut M, Borek B, et al. Elastic flow instabilities and macroscopic textures in graphene oxide lyotropic liquid crystals [J]. npj 2D Materials

and Applications, 2021, 5(11).

[35]Pott T, Meleard P. New insight into the nanostructure of ionic liquids: a small angle X-ray scattering (SAXS) study on liquid tri-alkyl-methyl-ammonium bis (trifluoromethanesulfonyl) amides and their mixtures [J]. Physical Chemistry Chemical Physics, 2009, 11(26): 5469-5475.

[36]Sartoratto P P C, Neto A V S, Lima E C D, et al. Preparation and electrical properties of oil-based magnetic fluids [J]. Journal of Applied Physics, 2005, 97(10).

[37]Öztürk N, Gökce H, Alpaslan G, et al. Structural, Spectroscopic (FT-IR, Raman, NMR and UV-Vis.) and Computational Studies on N-phenylpropanamide [J]. Journal of the Institute of Science and Technology, 2019, 823-834.

[38]Chen L, Liu J, Wang X, et al. Flexible Capacitive Hydrogel Tactile Sensor With Adjustable Measurement Range Using Liquid Crystal and Carbon Nanotubes Composites [J]. IEEE Transactions on Electron Devices, 2017, 64(5): 1968-1972.

[39]Du L, Yang X, Li W, et al. Construction of physical crosslink-based chitosan/liquid crystal composite hydrogel and evaluation on their cytocompatibility [J]. Regen Biomater, 2017, 4(1): 39-45.

[40]Joo H, Han H, Cho S. Fabrication of Poly(vinyl alcohol)-Polyaniline Nanofiber/Graphene Hydrogel for High-Performance Coin Cell Supercapacitor [J]. Polymers (Basel), 2020, 12(4): 928.

[41]Zhang W, Ma J, Zhang W, et al. A multidimensional nanostructural design towards electrochemically stable and mechanically strong hydrogel electrodes [J]. Nanoscale, 2020, 12(12): 6637-6643.

[42]Lai F, Fang Z, Cao L, et al. Self-healing flexible and strong hydrogel nanocomposites based on polyaniline for supercapacitors [J]. Ionics, 2020, 26(6): 3015-3025.

[43] Yin B-S, Zhang S-W, Ren Q-Q, et al. Elastic soft hydrogel supercapacitor for energy storage [J]. Journal of Materials Chemistry A, 2017, 5(47): 24942-24950.

[44] Soram B S, Dai J, Kshetri T, et al. Vertically grown and intertwined Co(OH)(2) nanosheet@Ni-mesh network for transparent flexible supercapacitor [J]. Chemical Engineering Journal, 2019, 123540(19): 32955-32959.

[45] Singh S B, Kshetri T, Singh T I, et al. Embedded PEDOT:PSS/AgNFs network flexible transparent electrode for solid-state supercapacitor [J]. Chemical Engineering Journal, 2019, 359:197-207.

[46] Zhu Y, Li N, Lv T, et al. Ag-Doped PEDOT:PSS/CNT composites for thin-film all-solid-state supercapacitors with a stretchability of 480% [J]. Journal of Materials Chemistry A, 2018, 6(3): 941-947.

[47] Manjakkal L, Pullanchiyodan A, Yogeswaran N, et al. A Wearable Supercapacitor Based on Conductive PEDOT:PSS-Coated Cloth and a Sweat Electrolyte [J]. Adv Mater, 2020, 32(24).

[48] Wang K, Zhang X, Li C, et al. Chemically Crosslinked Hydrogel Film Leads to Integrated Flexible Supercapacitors with Superior Performance [J]. Advanced Materials, 2015, 27(45): 7451-7457.

[49] Liu Q, Qiu J, Yang C, et al. High-Performance PVA/PEDOT:PSS Hydrogel Electrode for All-Gel-State Flexible Supercapacitors [J]. Advanced Materials Technologies, 2020, 6(1).

[50] Chu X, Zhao X, Zhou Y, et al. An ultrathin robust polymer membrane for wearable solid-state electrochemical energy storage [J]. Nano Energy, 2020, 76.

[51] Hu R, Zhao J, Jiang R, et al. Preparation of high strain polyaniline/polyvinyl alcohol composite and its applications in stretchable supercapacitor [J]. Journal of Materials Science: Materials in Electronics, 2017, 28(19): 14568-14574.

[52]F Cordobés J M, and C. Gallegos Linear Viscoelasticity of the Direct Hexagonal Liquid Crystalline Phase [J]. Journal of Colloid & Interface Science, 1997, 187(2): 401-417.